

# $^{22}\text{C}$ : An $S$ -Wave Two-Neutron Halo Nucleus

W. Horiuchi<sup>1</sup> and Y. Suzuki<sup>2</sup>

<sup>1</sup>*Graduate School of Science and Technology,  
Niigata University, Niigata 950-2181, Japan*

<sup>2</sup>*Department of Physics, and Graduate School of Science and Technology,  
Niigata University, Niigata 950-2181, Japan*

## Abstract

A dripline nucleus  $^{22}\text{C}$  is studied in a Borromean three-body model of  $^{20}\text{C}+n+n$ . The valence neutrons, interacting via a realistic potential, are constrained to be orthogonal to the occupied orbits in  $^{20}\text{C}$ . We obtain ample results supporting that  $^{22}\text{C}$  is an ideal  $S$ -wave two-neutron halo nucleus: The ground state is bound by 390-570 keV, the root mean square neutron and proton radii are 4.0 and 2.4 fm, and the two neutrons are predominantly in  $(s_{1/2})^2$  orbits. The binding mechanism of  $^{22}\text{C}$  is discussed. One- and two-body density distributions elucidate the halo character as well as the correlated motion of the neutrons. The reaction cross sections of  $^{22}\text{C}+^{12}\text{C}$  collisions are predicted.

PACS numbers: 27.30.+t, 21.10.Gv, 21.60.-n, 25.60.Dz

Keywords:  $^{22}\text{C}$ ; neutron halo; three-body model; density

The subshell closure of  $N=14$  and  $N=16$  is one of the topics discussed intensively in the study of neutron-rich nuclei, and the  $N=14$  closure has experimentally been confirmed around  $^{22}\text{O}$  [1, 2, 3, 4, 5]. This issue is closely related to the competition of  $0d_{5/2}$  and  $1s_{1/2}$  neutron orbits. In fact, they play a vital role in determining the ground state structure of  $A=15\text{--}20$  carbon isotopes. For example, the ground state of  $^{16}\text{C}$  is found to contain the  $(1s_{1/2})^2$  and  $(0d_{5/2})^2$  configurations nearly equally [6, 7], whereas the last neutron in  $^{19}\text{C}$  is in the  $1s_{1/2}$  orbit, forming one-neutron halo structure [8, 9]. The deformations of carbon isotopes are discussed to have a strong  $N$ -dependence [10, 11]. An overview of the structure of carbon isotopes is given in Ref. [12].

No information is available to determine whether the  $N=14$  subshell closure occurs in  $^{20}\text{C}$ . The systematics of the interaction cross section suggests, however, that the radius of  $^{20}\text{C}$  is smaller than that of  $^{19}\text{C}$  [13], so it is natural to assume that the ground state of  $^{20}\text{C}$  predominantly consists of a  $(0d_{5/2})^6$  configuration. If its dominant component were  $(0d_{5/2})^4(1s_{1/2})^2$ , one more neutron could be added to the  $0d_{5/2}$  orbit to form a particle-stable  $^{21}\text{C}$ , which is in contradiction to observation.

In this study we will demonstrate that  $^{22}\text{C}$  is an  $s$ -wave two-neutron halo nucleus on the basis of the analysis of its structure including the neutron and proton densities. For  $Z \leq 8$ ,  $^{22}\text{C}$  is an only dripline nucleus which the interaction or reaction cross section measurement on a  $^{12}\text{C}$  target has not reached yet [13], so it is of interest for a future measurement to predict the reaction cross section of  $^{22}\text{C}$ . The neutron and proton densities obtained here will be useful to estimate the reaction cross section of  $^{22}\text{C}$  on a proton target, which is being investigated experimentally [14]. Our model is that  $^{22}\text{C}$  is a three-body system of  $^{20}\text{C}+n+n$ , and that  $^{20}\text{C}$  has the  $(0d_{5/2})^6$  configuration.  $^{22}\text{C}$  is thus Borromean, just as  $^{11}\text{Li}$  is. Though  $^{22}\text{C}$  may be expected to be much like  $^{11}\text{Li}$  in its halo character, a remarkable difference will show up: In  $^{11}\text{Li}$  both of  $(0p_{1/2})^2$  and  $(1s_{1/2})^2$  components contribute to producing its halo [15, 16, 17], whereas in  $^{22}\text{C}$  only an  $(s_{1/2})^2$  component will be predominant. Another difference to be noted is that the  $^{20}\text{C}$  core has zero spin, which will make the content of angular momentum coupling in  $^{22}\text{C}$  simpler than that in  $^{11}\text{Li}$ .

The wave function for  $^{22}\text{C}$  is determined from the following Hamiltonian

$$H = T_{\lambda} + T_{\rho} + U_1 + U_2 + v_{12}, \quad (1)$$

where the subscripts,  $\lambda$  and  $\rho$ , of the kinetic energies stand for the relative distance vectors of the three-body system. The two-neutron potential  $v_{12}$  is taken from the realistic G3RS (case 1) potential [18] which contains central, tensor and spin-orbit forces and reproduces the nucleon-nucleon scattering data as well as the deuteron properties.  $U_i$  is the  $n\text{--}^{20}\text{C}$  potential whose form is assumed as

$$U = -V_0 f(r) + V_1 \ell \cdot \mathbf{s} \frac{1}{r} \frac{d}{dr} f(r) + V_s e^{-\mu r^2} \mathcal{P}_s, \quad (2)$$

where  $f(r)=[1+\exp(\frac{r-R_c}{a})]^{-1}$  with  $R_c=r_0 A_c^{1/3}$  ( $A_c=20$ ). The operator  $\mathcal{P}_s$  of the last term projects to the  $s$  wave of the  $n\text{--}^{20}\text{C}$  relative motion, so this term modifies the  $s$ -wave potential strength. To determine the parameters of  $U$ , we take into account the conditions that (i) the  $1s_{1/2}$  orbit is unbound as  $^{21}\text{C}$  is unstable for a neutron emission, and (ii) the  $0d_{5/2}$  orbit is bound by at most 2.93 MeV, which is the neutron separation energy of  $^{20}\text{C}$ . Without the  $\mathcal{P}_s$  term, the above conditions were barely met only by making  $V_1$  much larger than the standard strength [19]. The set A potential in Table I corresponds to this case. With the  $\mathcal{P}_s$  term included, we have more freedom to generate different potentials, which

TABLE I: Parameters of the  $n-^{20}\text{C}$  potential  $U$ .  $\mu=0.09\text{ fm}^{-2}$ .  $a$  and  $r_0$  are 0.6 fm and 1.3 fm for set A, while they are 0.65 fm and 1.25 fm for sets B, C and D.  $\varepsilon$  is the s.p. energy of the  $n-^{20}\text{C}$  relative motion. Energy and length are given in units of MeV and fm, respectively.

	$V_0$	$V_1$	$V_s$	$\varepsilon(0s_{1/2})$	$\varepsilon(0p_{3/2})$	$\varepsilon(0p_{1/2})$	$\varepsilon(0d_{5/2})$
set A	33.22	42.10	0.00	-19.03	-9.86	-4.77	-1.00
set B	43.24	25.63	9.46	-19.79	-14.32	-11.00	-2.93
set C	41.08	25.63	7.14	-19.56	-12.88	-9.58	-1.93
set D	38.76	25.63	4.66	-19.31	-11.37	-8.09	-0.93

offer the opportunity of investigating the sensitivity of  $U$  on theoretical results. The spin-orbit strength  $V_1$  is fixed to be the standard value. Three sets of  $U$  of this type are listed in Table I as B, C and D. These potentials are determined by giving different values for the  $0d_{5/2}$  single-particle (s.p.) energy: Set B potential gives the deepest energy, while set D the shallowest energy. The energies of the lower s.p. orbits turn out to be considerably different. It should be noted, however, that our result for  $^{22}\text{C}$  never depends on these energies but on their s.p. wave functions as will be seen later. Fortunately, the different potentials chosen here give almost the same s.p. wave function for each occupied orbit. All of the potentials are set to predict the  $1s_{1/2}$  s.p. energy almost zero. It may be probable that the  $s$ -wave potential strength is further weaker. In that case, the ground state energy of  $^{22}\text{C}$  which we will obtain below is to be considered a minimum.

The ground state of  $^{22}\text{C}$  is described as follows:

$$\Psi = \Phi_c \Phi_{2n}, \quad \text{with} \quad \Phi_{2n} = \sum_{i=1}^K C_i \Phi(\Lambda_i, A_i), \quad (3)$$

where  $\Phi_c$  is the intrinsic wave function of  $^{20}\text{C}$  and the valence neutron part  $\Phi_{2n}$  is given as a combination of correlated Gaussian bases

$$\Phi(\Lambda, A) = (1 - P_{12}) \left\{ e^{-\frac{1}{2} \tilde{\mathbf{x}} A \mathbf{x}} [[\mathcal{Y}_\ell(\mathbf{x}_1) \mathcal{Y}_\ell(\mathbf{x}_2)]_{L\chi_S(1,2)}]_{00} \right\}, \quad (4)$$

where  $P_{12}$  permutes the neutron coordinates and  $\tilde{\mathbf{x}} A \mathbf{x} = A_{11} \mathbf{x}_1^2 + 2A_{12} \mathbf{x}_1 \cdot \mathbf{x}_2 + A_{22} \mathbf{x}_2^2$ . The coordinates  $\mathbf{x}_1 = \boldsymbol{\rho} + \frac{1}{2} \boldsymbol{\lambda}$  and  $\mathbf{x}_2 = \boldsymbol{\rho} - \frac{1}{2} \boldsymbol{\lambda}$  are the distance vectors of the neutrons from the center of mass (c.m.) of  $^{20}\text{C}$ . The angular parts of the two-neutron motion are described using  $\mathcal{Y}_{\ell m}(\mathbf{r}) = r^\ell Y_{\ell m}(\hat{\mathbf{r}})$  and they are coupled with the spin part  $\chi_S$  to the total angular momentum zero. The basis function is specified by a set of angular momenta  $\Lambda = (\ell, S)$  ( $L=S$ ), and a  $2 \times 2$  symmetric matrix  $A$  ( $A_{21}=A_{12}$ ). The two neutrons are explicitly correlated due to the term  $A_{12} \mathbf{x}_1 \cdot \mathbf{x}_2$ , the inclusion of which assures a precise solution in a relatively small dimension [20].

It is vital to take into account the Pauli principle for the valence neutrons in determining the energy and corresponding wave function. Though the fulfillment of antisymmetrizing the core and valence neutrons is beyond the present model, the Pauli constraint is included by imposing that the valence neutrons cannot occupy any s.p. orbits  $u_{n\ell jm}$  of  $\Phi_c$ . Here  $u_{n\ell jm}$  are generated from  $U$ , and  $n\ell j$  runs over  $0s_{1/2}$ ,  $0p_{3/2}$ ,  $0p_{1/2}$ , and  $0d_{5/2}$ . We used the stochastic variational method (SVM) [20] to optimize the parameter matrices  $A$ . The

TABLE II: Properties of  $^{22}\text{C}$ . Length is given in units of fm.

	$E(\text{MeV})$	$R_{\text{rms}}^n$	$R_{\text{rms}}^p$	$R_{\text{rms}}^m$	$\sqrt{\langle x_1^2 \rangle}$	$\sqrt{\langle \rho^2 \rangle}$	$\sqrt{\langle \lambda^2 \rangle}$	$\langle \mathbf{x}_1 \cdot \mathbf{x}_2 \rangle$	$P_{S=0}$	$\langle (s_{1/2})^2 \rangle$
set A	-0.413	4.11	2.44	3.73	8.17	6.19	10.7	9.80	0.998	0.968
set B	-0.489	3.96	2.43	3.61	7.54	5.86	9.48	11.9	0.981	0.915
set C	-0.573	3.93	2.43	3.58	7.37	5.66	9.44	9.83	0.990	0.942
set D	-0.388	4.12	2.44	3.74	8.21	6.29	10.6	11.6	0.995	0.954

SVM increases the basis dimension one by one by testing a number of candidates which are chosen randomly. The basis selection with the SVM is very effective for taking care of the short-range repulsion of  $v_{12}$  as well as satisfying the orthogonality constraint.

The most important channel for the binding of  $^{22}\text{C}$  was found to be  $\Lambda=(0,0)$ , and other channels included were  $(1,0)$ ,  $(2,0)$ ,  $(1,1)$ , and  $(2,1)$ . Note, however, that our correlated basis functions in practice include higher partial waves as well. Convergent results are obtained with the basis dimension of  $K \approx 300$ . The  $U$ -dependence of the solution is moderate as shown in Table II. The result with the  $\ell$ -independent set A potential is similar to those with the other potentials, especially set D potential. This indicates that the present result is not very sensitive to the potential provided that it is chosen to satisfy the two conditions. The ground state energy is about  $-390$  to  $-570$  keV with respect to the  $^{20}\text{C}+n+n$  threshold, which is consistent with the empirical value of  $-0.423 \pm 1.140$  MeV [21]. In order to see the importance of both spatial and angular correlations of the basis functions, we repeated the following calculations. The first was to include only the single channel of  $\Lambda=(0,0)$ , and then the ground state energy turned out to be  $-0.29$  MeV for set B. In the second calculation which truncates the basis functions to those with  $\Lambda=(0,0)$  and  $A_{12}=0$  (no correlation calculation), we obtained the result that the ground state is bound by at most 90 keV. Thus the inclusion of the correlated bases is found to gain the energy of about 400 keV.

The rms neutron, proton and matter radii of  $^{22}\text{C}$ , assuming pointlike nucleons, are listed in Table II. They are obtained using the corresponding radii of  $^{20}\text{C}$ , 3.23, 2.37 and 2.99 fm, which are calculated from  $\Phi_c$ . The rms neutron radius is 3.9–4.1 fm. The rms matter radius results in about 3.6–3.7 fm, which corresponds to that of a stable nucleus with  $A \approx 60$ . Accordingly one may call  $^{22}\text{C}$  a giant halo nucleus. The probability of finding the spin-singlet neutrons,  $P_{S=0}$ , shows that the ground state of  $^{22}\text{C}$  almost consists of the  $S=0$  component. Therefore, the non-central potentials have small expectation values and play a minor role in binding  $^{22}\text{C}$ : In set B case, the value of  $\langle v_{12}(\text{tensor} + \text{spin-orbit}) \rangle$  is only 7 keV and that of  $\langle U_1(\text{spin-orbit}) \rangle$  is 57 keV. Thus the binding energy contribution virtually comes from the kinetic energy and the central potentials of both  $U$  and  $v_{12}$ .

It is interesting to understand how the Borromean system is bound. First of all, we note that the non-central forces are found to give negligible contributions. Rewriting the kinetic energy as  $T_{\lambda} + T_{\rho} = T_1 + T_2 + T_{\text{rc}}$  [22], where  $T_i$  is the kinetic energy for the  $n$ - $^{20}\text{C}$  relative motion and  $T_{\text{rc}}$  is the recoil correction term, we decompose the energy contribution as follows:

$$E = 2\langle T_1 + U_1 \rangle + \langle T_{\text{rc}} \rangle + \langle v_{12} \rangle. \quad (5)$$

The decomposition for set B case is  $2 \times (7.185 - 6.436) - 0.118 - 1.868 = -0.489$  MeV. Except for the small contribution of the  $\langle T_{\text{rc}} \rangle$  term, we conclude that the binding of  $^{22}\text{C}$  is obtained

by a delicate balance of the two factors: One is that the attraction of  $v_{12}$ , though not large, keeps the neutrons from separating, and the other is the weak attraction of  $U$  which puts the neutron in continuum.

We calculate the probability  $\langle(\ell_j)^2\rangle$  of finding the halo neutrons in an  $(\ell_j)^2$  component. The  $\langle(s_{1/2})^2\rangle$  value is listed in Table II. Other probabilities are, for set B case, 0.033, 0.024, 0.009, 0.007, 0.003, 0.003 for  $\ell_j=d_{3/2}, p_{3/2}, p_{1/2}, f_{7/2}, d_{5/2}, f_{5/2}$ , respectively. The other potential sets give similar results. We find that the  $(s_{1/2})^2$  component is predominant and many other components have small admixtures. Since no bound orbit exists for the valence neutron, a realistic shell-model description taking into account these components would be hard. On the contrary, the present approach has the advantage that it requires no s.p. energies, no matter how high the valence neutrons are excited.

The halo behavior of  $^{22}\text{C}$  is exhibited through the neutron density,  $\rho^n(\mathbf{r})$ , which is given by

$$\rho^n(\mathbf{r}) = \langle \Phi_{2n} | \rho_c^n(\frac{2}{22}\boldsymbol{\rho} + \mathbf{r}) | \Phi_{2n} \rangle + \rho_h(\mathbf{r}), \quad (6)$$

where  $\rho_c^n(\mathbf{r})$  stands for the intrinsic neutron density of  $^{20}\text{C}$ , which is calculated from  $\Phi_c$ , and  $\rho_h(\mathbf{r})$  is the halo-neutron density with respect to the c.m. of  $^{22}\text{C}$

$$\rho_h(\mathbf{r}) = \langle \Phi_{2n} | \sum_{i=1}^2 \delta(\mathbf{x}_i - \frac{2}{22}\boldsymbol{\rho} - \mathbf{r}) | \Phi_{2n} \rangle. \quad (7)$$

The integration of  $\rho_c^n$  in Eq. (6) takes care of the fluctuation of the c.m. of  $^{20}\text{C}$  around the c.m. of  $^{22}\text{C}$ . The proton density is given by

$$\rho^p(\mathbf{r}) = \langle \Phi_{2n} | \rho_c^p(\frac{2}{22}\boldsymbol{\rho} + \mathbf{r}) | \Phi_{2n} \rangle. \quad (8)$$

These densities are displayed in Fig. 1. The contribution of the halo density to  $\rho^n$  exceeds that of the core density beyond  $r=6.2$  fm. Note that  $\rho_h(\mathbf{r})/2$  is, roughly speaking, the

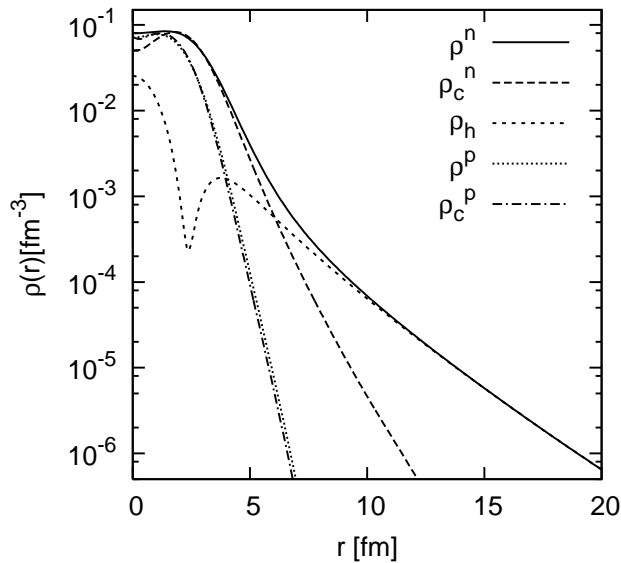


FIG. 1: The neutron and proton densities of  $^{22}\text{C}$  and  $^{20}\text{C}$ .  $\rho_h$  is the halo-neutron density. Set B potential is used.

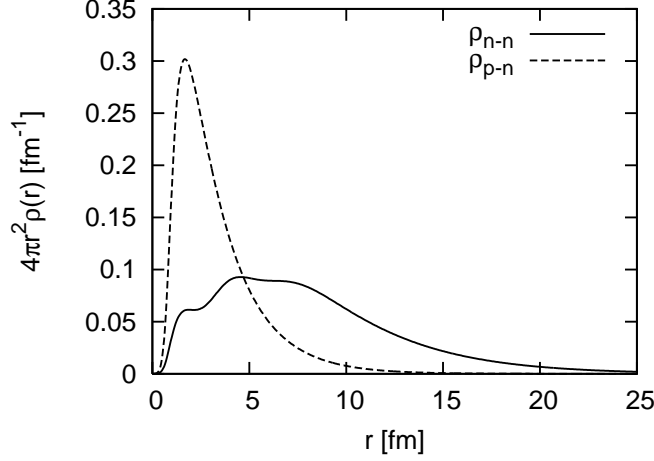


FIG. 2: Comparison of the two-body density distribution of the halo neutrons in  $^{22}\text{C}$  with that of the proton and neutron in the deuteron. Set B potential is used.

squared single halo-neutron wave function. The dip at around  $r=2.4$  fm is due to the orthogonality of  $\Phi_{2n}$  to the  $0s_{1/2}$  orbit.

It is of interest to examine the correlated motion of the two neutrons. A two-neutron subsystem with  $S = 0$  is often called a di-neutron when they have spatial extension comparable to that of the deuteron. The two-body halo-neutron distribution function,

$$\rho_{n-n}(\mathbf{r}) = \langle \Phi_{2n} | \delta(\boldsymbol{\lambda} - \mathbf{r}) | \Phi_{2n} \rangle, \quad (9)$$

is compared in Fig. 2 with the corresponding  $p-n$  distribution function of the deuteron

$$\rho_{p-n}(\mathbf{r}) = \frac{1}{3} \sum_{M=-1}^1 \langle \Phi_d(1M) | \delta(\mathbf{r}_p - \mathbf{r}_n - \mathbf{r}) | \Phi_d(1M) \rangle, \quad (10)$$

which is calculated using the G3RS potential. It is found that  $\rho_{n-n}(\mathbf{r})$  has a distribution much wider than  $\rho_{p-n}(\mathbf{r})$ . Thus the di-neutron correlation is not prominent in  $^{22}\text{C}$ . The value of  $\langle T_{\lambda} + v_{12} \rangle$  is 6.16 MeV (set B), which is to be compared to  $-2.28$  MeV (G3RS) of the deuteron. Since  $\rho_{n-n}(\mathbf{r})$  has a long tail, one may expect that the use of a two-nucleon potential with a one-pion exchange tail would give a potential energy different from the G3RS potential of a Gaussian tail. To check this point, we estimated the energy difference arising when the singlet-even central potential of G3RS is replaced with that of the OPEG potential (case 1) [18], using

$$\int d\mathbf{r} \rho_{n-n}(\mathbf{r}) [v_{12}(\text{OPEG}) - v_{12}(\text{G3RS})] \quad (11)$$

and found that the energy gain is only 6 keV.

Another function of interest is the two-neutron correlation function defined as

$$\rho(x_1, x_2, \theta) = \langle \Phi_{2n} | \Phi_{2n} \rangle_{\text{spin}}, \quad (12)$$

where  $\theta$  is the angle between  $\mathbf{x}_1$  and  $\mathbf{x}_2$  and  $\langle \cdots \rangle_{\text{spin}}$  indicates that the integration is to be done over the spin coordinates only. Figure 3 displays the value of  $8\pi^2 x^4 \sin\theta \rho(x, x, \theta)$ .

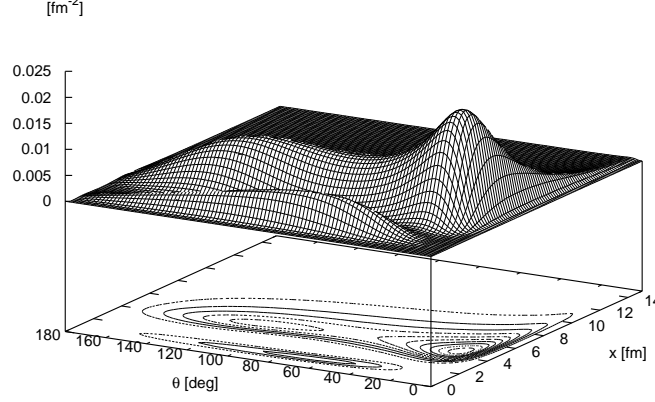


FIG. 3: The two-neutron correlation function  $\rho(x, x, \theta)$  weighted by  $8\pi^2 x^4 \sin\theta$ . The lower panel is its contour map. Set B potential is used.

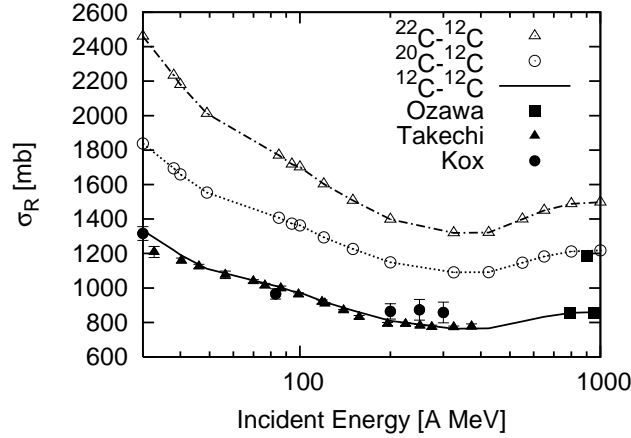


FIG. 4: Prediction of the reaction cross sections of  $^{22}\text{C}$  and  $^{20}\text{C}$  on a  $^{12}\text{C}$  target. Experimental data are taken from Refs. [13, 25, 26].

One prominent peak appears around  $x=5.0$  fm and  $\theta=17^\circ$ , which is often attributed to the correlation of di-neutron type, but the spatial extension of the two neutrons is too wide to be called the di-neutron, as shown in Fig. 2. The peak is followed by a plateau extending to larger angles. The valley of the correlation function which appears at around  $x=2.4$  fm reflects the dip observed in the halo-neutron density of Fig. 1.

The interaction cross section data for the carbon isotopes are available up to  $^{20}\text{C}$  for high incident energies [13]. With a reaction model proposed in Ref. [23], we predict the reaction cross section  $\sigma_R$  of  $^{22}\text{C}$  (and  $^{20}\text{C}$ ) using the calculated densities. To make the prediction reliable, we modify a nucleon-nucleon ( $NN$ ) profile function  $\Gamma_{NN}$  available in literatures [24] so as to reproduce both the elastic scattering cross section and the total cross section of the  $NN$  collision. Details will be published elsewhere. Figure 4 displays  $\sigma_R(^{12,20,22}\text{C})$  on a  $^{12}\text{C}$  target calculated at several incident energies. A good agreement between theory and experiment for  $\sigma_R(^{12}\text{C})$  confirms the validity of the modification of  $\Gamma_{NN}$ . The  $\sigma_R(^{20}\text{C})$  value at the incident energy of 900 A MeV is fairly well reproduced, which indicates that our model for  $\Phi_c$  is acceptable at least in its prediction for the radius of  $^{20}\text{C}$ . We thus expect

that  $\sigma_R(^{22}\text{C})$ , or at least the increase of the cross sections,  $\sigma_R(^{22}\text{C}) - \sigma_R(^{20}\text{C})$ , is predicted to good approximation. A measurement of  $\sigma_R(^{22}\text{C})$  for a wide range of incident energies will provide us with valuable information for quantifying the extent to which the halo reaches in far distances. We are studying the reaction cross section of  $^{22}\text{C}$  on a proton target as well.

To conclude, we studied the ground state structure of  $^{22}\text{C}$  in the  $^{20}\text{C}+n+n$  three-body model with the orthogonality constraint. The  $N=14$  subshell closure was assumed for  $^{20}\text{C}$ . We showed that  $^{22}\text{C}$  is an almost pure  $S$ -wave two-neutron halo nucleus, and that the non-central forces play no active role in binding this fragile system. A measurement of the reaction cross section of  $^{22}\text{C}+^{12}\text{C}$  is desired to establish the halo structure experimentally.

We thank A. Kohama for his interest and valuable discussions and M. Fukuda and M. Takechi for sending us the reaction cross section data of  $^{12}\text{C}+^{12}\text{C}$ . This work was in part supported by a Grant for Promotion of Niigata University Research Projects (2005-2007).

- 
- [1] A. Ozawa, T. Kobayashi, T. Suzuki, K. Yoshida and I. Tanihata, Phys. Rev. Lett. **84**, 5493 (2000).
  - [2] P. G. Thirolf *et al.*, Phys. Lett. B **485**, 16 (2000).
  - [3] D. Cortina-Gil *et al.*, Phys. Rev. Lett. **93**, 062501 (2004).
  - [4] M. Stanoiu *et al.*, Phys. Rev. C **69**, 034312 (2004).
  - [5] E. Becheva *et al.*, Phys. Rev. Lett. **96**, 012501 (2006).
  - [6] T. Yamaguchi *et al.*, Nucl. Phys. **A724**, 3 (2003).
  - [7] W. Horiuchi and Y. Suzuki, Phys. Rev. C **73**, 037304 (2006).
  - [8] T. Nakamura *et al.*, Phys. Rev. Lett. **83**, 1112 (1999).
  - [9] V. Maddalena *et al.*, Phys. Rev. C **63**, 024613 (2001).
  - [10] Y. Kanada-En'yo, Phys. Rev. C **71**, 014310 (2005).
  - [11] H. Sagawa, X. R. Zhou, X. Z. Zhang and T. Suzuki, Phys. Rev. C **70**, 054316 (2004).
  - [12] B. A. Brown, Prog. Part. Nucl. Phys. **47**, 517 (2001).
  - [13] A. Ozawa, T. Suzuki and I. Tanihata, Nucl. Phys. A **693**, 32 (2001).
  - [14] K. Tanaka *et al.*, private communication.
  - [15] I. J. Thompson and M. V. Zhukov, Phys. Rev. C **49**, 1904 (1994).
  - [16] H. Simon *et al.*, Phys. Rev. Lett. **83**, 496 (1999).
  - [17] K. Varga, Y. Suzuki and R. G. Lovas, Phys. Rev. C **66**, 041302(R) (2002).
  - [18] R. Tamagaki, Prog. Theor. Phys. **39**, 91 (1968).
  - [19] A. Bohr and B. R. Mottelson, *Nuclear Structure*, Vol. I (Benjamin, New York, 1969).
  - [20] K. Varga and Y. Suzuki, Phys. Rev. C **52**, 2885 (1995); Y. Suzuki and K. Varga, *Stochastic Variational Approach to Quantum-Mechanical Few-Body Problems*, Lecture notes in physics, Vol. m54 (Springer, Berlin, 1998).
  - [21] G. Audi, A. H. Wapstra and C. Thibault, Nucl. Phys. A **729**, 337 (2003).
  - [22] Y. Suzuki and K. Ikeda, Phys. Rev. C **38**, 410 (1988).
  - [23] B. Abu-Ibrahim and Y. Suzuki, Phys. Rev. C **61**, 051601(R) (2000); *ibid.* C **62**, 034608 (2000).
  - [24] L. Ray, Phys. Rev. C **20**, 1857 (1979). S. M. Lenzi, A. Vitturi and F. Zardi, Phys. Rev. C **40**, 2114 (1989).
  - [25] M. Takechi *et al.*, Euro. Phys. J. A **25**, s01, 217 (2005) and private communication.
  - [26] S. Kox *et al.*, Phys. Rev. C **35**, 1678 (1987).